25th ABCM International Congress of Mechanical Engineering
October 20-25, 2019, Uberlândia, MG, Brazil

COB-2019-1274
HYBRID-TREFFTZ FINITE ELEMENT LINEAR ISOTROPIC ANALYSIS WITH NON-ORTHOGONAL TRIAL FUNCTIONS

Felipe Alvarez Businaro
Flávio Luiz da Silva Bussamra
Instituto Tecnológico de Aeronáutica, 12228 − 900 São José dos Campos, SP, Brazil
businaro@ita.br; flaviobu@ita.br;

Abstract. *This paper proposes the use of non-orthogonal trial functions in the analysis of finite element benchmark tests modeled with the Hybrid-Trefftz stress element formulation. The elements are built in the generalized form instead of using the conventional nodal setup, in order to allow an easy –p refinement of the approximation field functions. The formulation chosen for this paper approximates the stresses in the domain and the displacements in the boundary, independently. Since this kind of finite element formulation generates very rich elements with a high number of degrees of freedom, orthogonal functions have been used to interpolate the field approximations in order to produce a high sparsity solving system matrix. However, this paper aims to demonstrate that good results can be attained by deriving a set of trial functions from a homogeneous polynomial harmonic potential. Results from convergence analysis and mesh distortion are shown, while comparing to the more conventional Legendre-Chebyshev orthogonal functions.*

Keywords: *Hybrid-Trefftz, stress element, linear isotropic, finite element, non-orthogonal*

1. INTRODUCTION

The hybrid-Trefftz formulation used in this work was developed by Freitas (1998), Freitas et al. (1999) and his colleagues in a number of papers (Freitas and Bussamra, 2000; Bussamra et al., 2001, 2012, 2014, 2016). This formulation is based on the pioneering work of Pian (1964), Pian and Tong (1969) and Fraejis de Veubeke (1980) as an alternative to the single field displacement element that is widely spread nowadays. The hybrid element consists in independent approximations of the domain and boundary fields. Since it is a stress version of that element, the stresses are approximated in the domain, and the displacements in the boundaries.

In this paper, a harmonic homogeneous polynomial potential (Wang et al., 2012) is going to be used to derive the field functions through the Papkovitch-Neuber (Papkovich, 1932; Neuber, 1934) solution of Navier's equation of equilibrium for isotropic materials. This set of functions is hierarchical, and when compared to the usual Legendre-Chebyshev associated potential used by Freitas and his colleagues it has the advantage of being complete in any desired level of approximation.

Hybrid-Trefftz elements have been applied with good results in the analysis of elastostatic (Freitas and Bussamra, 2000) and elastoplastic (Bussamra et al., 2001) problems, in crack analysis and simulation singular stress fields (Bussamra *et al.*, 2014; de Souza and Proença, 2011; Lee *et al.* 2010). It can be also mentioned the applications in 2D cohesive crack propagation with geometric nonlinearities (Kaczmarczyk and Pearce, 2009) and in multisite cracked solids (de Argôlo and Proença, 2017).

Some examples of the use of Hybrid-Trefftz elements outside linear elastic mechanics can be cited aswell. Fu et al. (2011) analyzed heat conduction in functionally graded nonlinear anisotropic materials using a nodal Hybrid-Trefftz element; Cao et al. (2013) used complex variables derived from Muskhelishvili to approximate the domain fields when analyzing micromechanics of heterogeneous composites. Petrolito (2004) used bi-harmonic polynomials as approximation functions implemented in triangular elements with Hybrid-Trefftz formulation to analyze stability and buckling of thick and thin 2D plates, and later studied vibration and stability on thick orthotropic plates (Petrolito, 2014). Karkon and Rezaiee-Pajand (2012, 2014, 2016) studied, respectively, plate bending, thin plate bending with high order elements and thick orthotropic plates, but in rectangular and triangular elements with a different set of trial functions at the boundaries. Karkon (2015) also proposed rectangular and triangular elements to analyze anisotropic laminated plates.

2. FORMULATION

The Hybrid-Trefftz formulation is developed from the basic linear elastic fundamental governing equations, being applied to a domain V and a boundary Γ, referred to a Cartesian coordinate system:

$$\mathbf{D}\boldsymbol{\sigma} + \bar{\mathbf{b}} = \mathbf{0}, \text{ in V} \tag{1}$$

$$\boldsymbol{\varepsilon} = \mathbf{D^*}\,\mathbf{u}, \text{ in V} \tag{2}$$

$$\boldsymbol{\varepsilon} = \mathbf{f}(\boldsymbol{\sigma} - \bar{\boldsymbol{\sigma}}_{\boldsymbol{\theta}}) + \bar{\boldsymbol{\varepsilon}}_{\boldsymbol{\theta}}, \text{ in V} \tag{3}$$

$$\mathbf{N}\boldsymbol{\sigma} = \bar{\mathbf{t}}_{\Gamma}, \text{ in } \Gamma_{\boldsymbol{\sigma}} \tag{4}$$

$$\mathbf{u} = \bar{\mathbf{u}}_{\Gamma}, \text{ in } \Gamma_{\mathbf{u}} \tag{5}$$

Where vector $\boldsymbol{\sigma}$ and ε collect the independent terms of the stress tensor in the equilibrium equation Eq. (1) and the strain tensor in the compatibility equation Eq. (2), respectively. $\bar{\boldsymbol{b}}$ and $\boldsymbol{u}$ represents the prescribed body forces vector and displacement vector, respectively. $\boldsymbol{f}$ represents the flexibility format of the constitutive equation Eq. (3) which is symmetric and with constant entries when a linear, reciprocal law is assumed. $\bar{\boldsymbol{\sigma}}_{\boldsymbol{\theta}}$ and $\bar{\boldsymbol{\varepsilon}}_{\boldsymbol{\theta}}$ represents the residual stresses and strains vector, respectively, but for simplicity $\bar{\boldsymbol{\sigma}}_{\boldsymbol{\theta}}$, $\bar{\boldsymbol{\varepsilon}}_{\boldsymbol{\theta}}$ and $\bar{\boldsymbol{b}}$ will be set to zero. Equation (4) represents the Neumann boundary condition applied in the static section of the boundary (Γ_{σ}), where $\bar{\boldsymbol{t}}_{\boldsymbol{\Gamma}}$ stands for the prescribed tractions vector. Equation (5) represents the Dirichlet boundary condition, applied to the kinematic portion of the boundary (Γ_{u}), where $\bar{\boldsymbol{u}}_{\boldsymbol{\Gamma}}$ stands for the prescribed displacements. $\boldsymbol{D}$ is the differential equilibrium operator and $\boldsymbol{D^*}$ is the compatibility operator. Both are linear and adjoint in the context of geometrically linear models. Matrix $\boldsymbol{N}$ contains the unit outward normal vector associated with the operator $\boldsymbol{D}$.

2.1 Approximation fields

The Hybrid-Trefftz element approximates one field in the domain and one field in the boundary, independently. Since this work proposes to use the stress version of this formulation, the generalized stresses are going to be directly approximated in the domain, and the displacements in the boundary.

$$\boldsymbol{\sigma} = \mathbf{S}\mathbf{X} \tag{6}$$

$$\mathbf{u}_{\Gamma} = \mathbf{Z}\mathbf{q} \tag{7}$$

Where $\boldsymbol{S}$ and $\boldsymbol{Z}$ are matrices that collect the approximation functions and $\boldsymbol{X}$ and $\boldsymbol{q}$ are their associated generalized stresses and displacements, respectively.

2.2 Trefftz constraint

By requiring the domain stress approximation Eq. (6) to satisfy locally the system of differential equations that govern the problem, the Trefftz constraint is enforced, resulting in the following condition:

$$\mathbf{D}\mathbf{S} = \mathbf{0}, \text{ in V} \tag{8}$$

Meaning $\boldsymbol{S}$ must be a self-equilibrated field. It is possible to relate the equilibrium Eq. (1) and compatibility Eq. (2) equations to write it in terms of displacement, substituting Eq. (2) and the constitutive relation Eq. (3) (written in terms of rigidity) into Eq. (1). The result follows:

$$\boldsymbol{\sigma} = \mathbf{k}\mathbf{D}^{\mathbf{T}}\mathbf{u}, \text{ in V} \tag{9}$$

$$\mathbf{D}\mathbf{k}\mathbf{D}^{\mathbf{T}}\mathbf{u} = \mathbf{0}, \text{ in V} \tag{10}$$

Therefore, $\boldsymbol{S}$ is directly compatible with the domain displacement $\boldsymbol{u}$. Considering now the following approximation to the domain displacement $\boldsymbol{u}$, where $\boldsymbol{U}$ is the matrix that collects the associated functions of the displacement basis, $\boldsymbol{X}$ is the generalized displacement vector and $\boldsymbol{u}_{\boldsymbol{\Gamma}}$ is the vector that collects the rigid-body motion.

$$\mathbf{u} = \mathbf{U}\mathbf{X} + \mathbf{u}_{\Gamma} \tag{11}$$

Substituting Eqs. (6 and 11) into Eq. (9), the stress approximation basis of the domain is defined.

$$\mathbf{S} = \mathbf{k}\mathbf{D}^{\mathbf{T}}\mathbf{U} \tag{12}$$

3. ON THE CHOICE OF U

In the literature, it is possible to find some analytic solution to the three-dimensional elasticity fundamental equation, like the quasi Hu Hai-Chang (Hu, 2008), Boussinesq-Galerkin (Wang, 2002) and Papkovitch-Neuber. However, Fu et al. (2012) presents an argument that only a modified version of the Papkovitch-Neuber is able to directly formulate a linear independent and complete set of displacement approximation functions. For this reason, the Papkovitch-Neuber solution will be used in this work.

Papkovitch (1932) and Neuber (1934) proposed independently, for an isotropic material, a three-dimensional solution of the Navier equation Eq. (10).

$$2G\mathbf{u} = -4(1-\nu)\boldsymbol{\Psi} + \nabla(\mathbf{r}\boldsymbol{\Psi} + \phi) \tag{13}$$

Where $\boldsymbol{\Psi}$ and ϕ are a vector and scalar harmonic displacement potential, respectively. G represents the shear modulus, $\boldsymbol{r}$ the position vector, ν the Poisson ratio and ∇ is the gradient operator.

Naghdu and Hsu (1961), Mindlin (1936) and some other authors proved that the Papkovitch-Neuber solution is complete, but some field representations can be redundant which means the results must be scanned for linear dependencies. In order to eliminate these dependencies Eubanks and Sternberg (1956), Sokolnikoff (1956), Naghdu and Hsu (1961) and Cong and Steven (1979) show and prove that given the specific conditions the scalar potential ϕ can be dropped without any loss to completeness. Since the three-dimensional element used in this work is a star-shaped hexagon and 4ν will not be an integer in the numerical examples shown in this work, the necessary conditions to drop ϕ are met. Therefore, if the vector $\boldsymbol{\Psi}$ is harmonic, Eq. (13) becomes:

$$2G\mathbf{u} = -4(1-\nu)\boldsymbol{\Psi} + \nabla(\mathbf{r}\boldsymbol{\Psi}) \tag{14}$$

3.1 Homogeneous harmonic polynomials potential

Generated through Pascal's trinomial distribution, this set of functions contain all possible polynomial combinations hence the reason it is a complete set. Following the work of Wang (2012) it is possible to transform the result from the trinomial distribution into the harmonic set by applying the Laplace operator, since this is the condition for a polynomial to be harmonic. Then, through a substitution procedure, the dependencies are eliminated. The resulting linear independent terms are separated to build the approximation set, as is thoroughly explained in Wang's work.

It is worth to mention that once the approximation set is built, their terms are always linear independent, even after passing through the Papkovitch-Neuber solution. Therefore, no further search for dependencies is necessary.

4. FINITE ELEMENT MATRICES

Freitas (1998) and Bussamra et al. (2001) stated different approaches could be pursued to define the finite element equations from the presented fundamental relations for linear elasticity Eq. (1-5) and the field approximations Eq. (6 and 7), namely the principle of virtual work, duality and well-established variational statements. In this work, the virtual work approach presented below will be used.

$$\int \boldsymbol{\sigma}^{\mathrm{T}}\boldsymbol{\varepsilon}\, \mathrm{dV} = \int \mathbf{b}^{\mathrm{T}}\mathbf{u}\, \mathrm{dV} + \int \mathbf{t}^{\mathrm{T}}\mathbf{u}\, \mathrm{d}\Gamma_{\boldsymbol{\sigma}} + \int \mathbf{u}^{\mathrm{T}}\mathbf{t}\, \mathrm{d}\Gamma_{\mathrm{u}} \tag{15}$$

As previously mentioned, the body forces vector will be considered null in this work. Substituting the static and kinematic boundary conditions Eq. (4) and Eq. (5), respectively, in Eq. (15), and then taking the first variation in terms of the generalized stress results in:

$$\int \delta\boldsymbol{\sigma}^{\mathrm{T}}\boldsymbol{\varepsilon}\, \mathrm{dV} = \int (\mathbf{N}\,\delta\boldsymbol{\sigma})^{\mathrm{T}}\,\mathbf{u}\, \mathrm{d}\Gamma_{\boldsymbol{\sigma}} + \int (\mathbf{N}\,\delta\boldsymbol{\sigma})^{\mathrm{T}}\bar{\mathbf{u}}_{\Gamma}\, \mathrm{d}\Gamma_{\mathrm{u}} \tag{16}$$

In sequence, the stress and boundary displacement approximations, Eq. (6) and Eq. (7) respectively, into Eq. (16). The unknown variable of Eq. (16) will be $\boldsymbol{X}$, which is the one that suffers variation form now on. However, it is not the trivial solution that is being pursued, meaning $\boldsymbol{\delta X} \neq \boldsymbol{0}$. Thus, substituting the constitutive relation given by Eq. (3):

$$\left(\int \mathbf{S}^{\mathrm{T}}\mathbf{f}\ \mathbf{S}\ \mathrm{dV}\right)\delta\mathbf{X} = \left(\int (\mathbf{NS}\,\delta\mathbf{X})^{\mathrm{T}}\ \mathbf{Z}\ \mathrm{d}\Gamma_{\boldsymbol{\sigma}}\right)\mathbf{q} + \int (\mathbf{NS}\,\delta\mathbf{X})^{\mathrm{T}}\,\bar{\mathbf{u}}_{\Gamma}\ \mathrm{d}\Gamma_{\mathrm{u}} \tag{17}$$

Equation (16) can be represented in the following form:

$$\mathbf{FX} - \mathbf{Aq} = \mathbf{v} \tag{18}$$

Where,

$$\mathbf{F} = \int_{\mathrm{V}} \mathbf{S}^{\mathrm{T}}\mathbf{f}\ \mathbf{S}\ \mathrm{dV} \tag{19}$$

$$\mathbf{A} = \int_{\Gamma_{\boldsymbol{\sigma}}} (\mathbf{NS})^{\mathrm{T}}\ \mathbf{Z}\ \mathrm{d}\Gamma \tag{20}$$

$$\mathbf{v} = \int_{\Gamma_{\mathrm{u}}} (\mathbf{NS})^{\mathrm{T}}\,\bar{\mathbf{u}}_{\Gamma}\ \mathrm{d}\Gamma \tag{21}$$

The Neumann boundary condition Eq. (4) is directly enforced to guarantee the stress continuity condition, which is the typical condition of a stress element, as shown below.

$$\int_{\Gamma_{\sigma}} \delta\mathbf{u}^{\mathrm{T}}\mathbf{N}\boldsymbol{\sigma}\ \mathrm{d}\Gamma = \int_{\Gamma_{\sigma}} \delta\mathbf{u}^{\mathrm{T}}\,\bar{\mathrm{t}}_{\Gamma}\ \mathrm{d}\Gamma \tag{22}$$

Substituting the boundary displacement approximation Eq. (8) into Eq. (22) results in:

$$-\mathbf{A}^{\mathrm{T}}\mathbf{X} = -\mathbf{Q} \tag{23}$$

Where,

$$\mathbf{Q} = \int_{\Gamma_{\sigma}} \mathbf{Z}^{\mathrm{T}}\,\bar{\mathrm{t}}_{\Gamma}\ \mathrm{d}\Gamma \tag{24}$$

Equations (18) and (23), along with (21) and (24), represent the structure solving system and can be grouped and shown in matrix form.

$$\begin{bmatrix} \mathbf{F} & -\mathbf{A} \\ -\mathbf{A}^{\mathrm{T}} & 0 \end{bmatrix} \begin{Bmatrix} \mathbf{X} \\ \mathbf{q} \end{Bmatrix} = \begin{Bmatrix} \mathbf{v} \\ -\mathbf{Q} \end{Bmatrix} \tag{25}$$

Vectors ***v*** and ***Q*** vary with element geometry due to the prescribed displacements and tractions, respectively, being assigned to the surfaces. The stress basis ***S*** contains the individual function sets for each degree of approximation, up to degree *n*. Therefore, the matrix ***S*** used in Eq. (19-21) are of the following format, with $\boldsymbol{S_0}$ being a 6 by 6 identity matrix.

$$\mathbf{S} = \left[\ \mathbf{S}_0, \mathbf{S}_1, \mathbf{S}_2, \ldots, \mathbf{S}_n\ \right] \tag{26}$$

Matrix ***Z*** contains the boundary displacement approximation basis defined in Eq. (7). It is built from hierarchical polynomial terms, defined in each face's local coordinates (ξ_1, ξ_2) according to Pascal's pyramid distribution.

$$\begin{array}{ccccccc} & & & 1 & & & \\ & & \xi_1 & & \xi_2 & & \\ & \xi_1^2 & & \xi_1\xi_2 & & \xi_2^2 & \\ \xi_1^3 & & \xi_1^2\xi_2 & & \xi_1\xi_2^2 & & \xi_2^3 \end{array}$$

Figure 1. Pascal's binomial distribution for a Cartesian (ξ_1, ξ_2) system located at each element's faces, up to degree 3.

Considering n as the boundary displacement degree, the number of approximation fields is given by Eq. (27).

$$n_Z = 3\left[\frac{1}{2}(n+1)(n+2)\right] \tag{27}$$

For $n = 2$, $\mathbf{Z}$ has the following fields:

$$\mathbf{Z} = \begin{bmatrix} \mathbf{Z}_x & 0 & 0 \\ 0 & \mathbf{Z}_y & 0 \\ 0 & 0 & \mathbf{Z}_z \end{bmatrix} = \begin{bmatrix} 1 & \xi_1 & \xi_2 & \xi_1^2 & \xi_1\xi_2 & \xi_2^2 & 0 & 0 & 0 & 0 & 0 & 0 & 0 & 0 & 0 & 0 & 0 & 0 \\ 0 & 0 & 0 & 0 & 0 & 0 & 1 & \xi_1 & \xi_2 & \xi_1^2 & \xi_1\xi_2 & \xi_2^2 & 0 & 0 & 0 & 0 & 0 & 0 \\ 0 & 0 & 0 & 0 & 0 & 0 & 0 & 0 & 0 & 0 & 0 & 0 & 1 & \xi_1 & \xi_2 & \xi_1^2 & \xi_1\xi_2 & \xi_2^2 \end{bmatrix} \tag{28}$$

These fields represent a face with no constraints. In order to eliminate a displacement degree of freedom from the face to represent a simply supported case, for instance, only one of the directions may be eliminated from matrix $\mathbf{Z}$. In case of a clamped face, where movement in the three directions are restricted, the whole face is left out of the calculations and it is not accounted for in Eq. (20) nor in Eq. (24). This approximation does not satisfy face-to-face and edge continuity between elements. This effect is lessened as the exact solution is approached. An advantage of having this non-conformity is the higher continuity obtained in the stresses, which is desired in a stress element (Freitas, 1997).

5. NUMERICAL IMPLEMENTATION

According to Freitas et al. (1999), the Hybrid-Trefftz approximation bases are strongly constrained since they are required to satisfy the governing problem's differential equation, which in the case of this work are the equilibrium and compatibility equations Eqs. (1 and 2). This result in a Finite Element Method (FEM) modelling that is very rich in information about the phenomenon being modelled and a high accuracy with relatively few degrees of freedom. The solving system, besides being small in dimension, is free from spurious modes and is well conditioned.

The integration procedures were realized by the Gauss Quadrature method, both for volume and surface integrals. There are no restrictions in the degree of approximation since it is possible to obtain points and weights for any desired degree, as shown vastly in the numerical methods literature. However, in order to minimize the numerical error and improve efficiency, the polynomial equations were integrated using the least number of Gauss points that would render an exact integration.

5.1 Coordinate transformation

The chosen element geometry for this work is hexahedrical, and in order to map the mesh of elements an isoparametric master element of 8 nodes is used. Its natural coordinates are defined in terms of [q, r, t] and the coordinate transformation is done through a set of trilinear isoparametric equations given by Eq. (29).

$$\Phi_i = \frac{1}{8}(1+q_i q)(1+r_i r)(1+t_i t), \qquad i = 1, \ldots, 8 \tag{29}$$

Where q_i, r_i and t_i are the ith node coordinates of the master element. These functions are applied acoording to Eq. (30), where $\boldsymbol{x}_{master}$ are the master element's natural coordinates that range from -1 to 1; and $\boldsymbol{x}_{local}$ are the coordinates of each element, according to its local system. This local coordinate system is defined using each element's centroid as origin, which is required in order to improve the sparsity of the solving system, as mentioned in Bussamra et al. (2012, 2014).

$$\mathbf{x}_{local} = \boldsymbol{\Phi}\,\mathbf{x}_{master} \tag{30}$$

Therefore, for a given element, Eq. (19) becomes

$$\mathbf{F}_e = \int_{-1}^{1}\int_{-1}^{1}\int_{-1}^{1} \mathbf{S}_e^T \mathbf{f}\, \mathbf{S}_e \left|\mathbf{J}\right| dqdrdt \tag{31}$$

Where $\boldsymbol{S}_e = \boldsymbol{S}(x(q,r,t), y(q,r,t), z(q,r,t))$; and $\boldsymbol{J}$ is the jacobian matrix of transformation given by Eq. (30).

The $\boldsymbol{F}$ matrix present in Eq. (25) is a square, block diagonal matrix that contains each element's individual $\boldsymbol{F}_e$ matrix. This means each element's $\boldsymbol{F}_e$ matrix is independent, making it possible to implement parallel computational routines to calculate them more time efficiently, being this one of the advantages of the Hybrid elements formulations when compared to conventional commercial FEM applications.

5.2 Surface integrals over faces

Now, consider the following face organization of a given element, according to Figure 2.

Face 1: $q = -1,\ \xi_1 = r,\ \xi_2 = t$

Face 2: $q = 1,\ \xi_1 = r,\ \xi_2 = t$

Face 3: $\xi_1 = q,\ \xi_2 = r,\ t = -1$

Face 4: $\xi_1 = q,\ r = 1,\ \xi_2 = t$

Face 5: $\xi_1 = q,\ \xi_2 = r,\ t = 1$

Face 6: $\xi_1 = q,\ r = -1,\ \xi_2 = t$

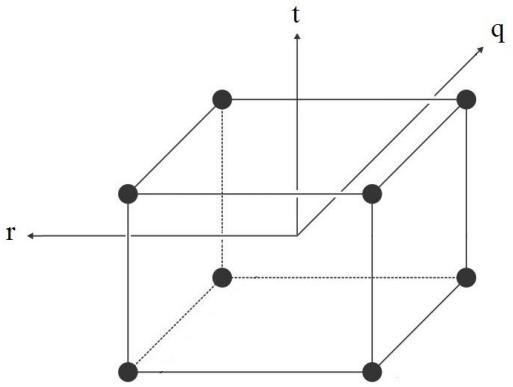

Figure 2. Face disposition on hexahedric master element.

In the master element, the unit normal vectors pointing outwards from the faces are given by Eq. (32).

$$\tilde{\mathbf{n}}_1 = \begin{Bmatrix} -1 \\ 0 \\ 0 \end{Bmatrix};\ \tilde{\mathbf{n}}_2 = \begin{Bmatrix} 1 \\ 0 \\ 0 \end{Bmatrix};\ \tilde{\mathbf{n}}_3 = \begin{Bmatrix} 0 \\ 0 \\ -1 \end{Bmatrix};\ \tilde{\mathbf{n}}_4 = \begin{Bmatrix} 0 \\ 1 \\ 0 \end{Bmatrix};\ \tilde{\mathbf{n}}_5 = \begin{Bmatrix} 0 \\ 0 \\ 1 \end{Bmatrix};\ \tilde{\mathbf{n}}_6 = \begin{Bmatrix} 0 \\ -1 \\ 0 \end{Bmatrix} \tag{32}$$

Therefore, the normal vectors of each element can be obtained through Eq. (33). Matrix $\boldsymbol{N}$ is the normal operator related to the differential operator $\boldsymbol{D}$ and is formed according to Eq. (34).

$$\mathbf{n}_i = \begin{Bmatrix} n_{x_i} \\ n_{y_i} \\ n_{z_i} \end{Bmatrix} = \mathbf{J}^{-1} \left|\mathbf{J}\right| \tilde{\mathbf{n}}_i, \quad i = 1, \ldots, 6 \tag{33}$$

$$\mathbf{N}_i = \begin{bmatrix} n_{x_i} & 0 & 0 & 0 & n_{z_i} & n_{y_i} \\ 0 & n_{y_i} & 0 & n_{z_i} & 0 & n_{x_i} \\ 0 & 0 & n_{z_i} & n_{y_i} & n_{x_i} & 0 \end{bmatrix}, \quad i = 1, \ldots, 6 \tag{34}$$

The surface integrals composing matrices $\boldsymbol{A}$, $\boldsymbol{Q}$ and $\boldsymbol{v}$ must be calculated in each unconstrained face, and in case of a partial restriction, in each unconstrained direction. When a face is shared by two elements, it is accounted for only one time as an available face, but it must be calculated two times, due to the normal $\boldsymbol{N}$ being different.

As an example, calculating Eqs. (20, 21 and 24) for face 3 results in:

$$\mathbf{A} = \int_{-1}^{1}\int_{-1}^{1} (\mathbf{N}_3\mathbf{S}_e)^T\, \mathbf{Z}_e \ \mathrm{d}q\mathrm{d}r \tag{35}$$

$$\mathbf{v} = \int_{-1}^{1}\int_{-1}^{1} (\mathbf{N}_3\mathbf{S}_e)^T \bar{\mathbf{u}}_{\Gamma_3} \mathrm{d}q\mathrm{d}r \tag{36}$$

$$\mathbf{Q} = \int_{-1}^{1}\int_{-1}^{1} \mathbf{Z}_e{}^T\, \bar{\mathrm{t}}_{\Gamma_e} \left\|\mathbf{n}_3\right\| \mathrm{d}q\mathrm{d}r \tag{37}$$

It is worth to mention that for an element with distorted shape when compared to the master element, $\boldsymbol{J}$ and $\boldsymbol{N}_i$ can be a function of the local coordinates [q, r, t].

5.3 Solving system example

Consider a beam composed of 2 elements with both ends fixed, and a distributed load in its top surfaces (for this example, consider the top faces to be faces 4 and 8). The solving system, Eq. (25), for this case is assembled in the following manner, according to Fig. 3.

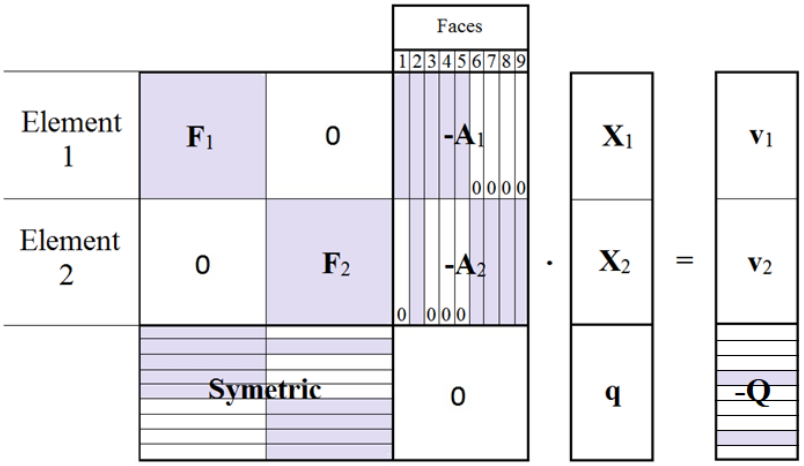

Figure 3. Solving system for a 2-element beam with fixed ends. Shaded parts represent non-null sub-matrices.

6. RESULTS

The following tests are performed in order to verify the accuracy of the presented non-orthogonal approximation basis in terms of linear elastic analysis, and its convergence properties. The results are compared with conventional conforming displacement elements, and with the Legendre-Chebyshev associated orthogonal potentials of Bussamra et al. (2014, 2001) and Freitas and Bussamra (2000).

6.1 Convergence analysis

Consider a beam with elastic modulus E = 1 and Poisson's coefficient $v = 0.2$. It has both ends clamped, square section of size 0.2L and length of L. It is subject to a uniformly distributed load in its superior face of magnitude q. Both -p and -h refinements were tested. The results shown in Tab. 1 were normalized by v = 5.509qL/E, which is the displacement of the lower face at the center of the beam. This value was obtained using a commercial FEM software, with a model of 22.500 quadratic hexahedric displacement elements.

Each mesh presented in Fig. 4 was evaluated with five combinations of approximations, given by [d_V , d_Γ], where d_V and d_Γ are the degree of approximation in the domain and in the boundary, respectively.

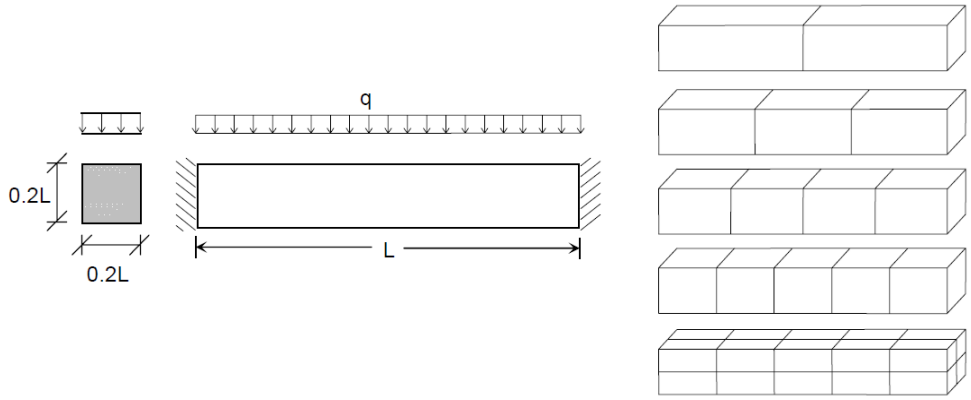

Figure 4. (Left) Beam with both ends fixed under uniform load. (Right) Mesh with 2, 3, 4, 5, 20 elements.

Table 1. Convergence analysis of a bi-clamped beam.

Number of elements	Homogeneous Harmonic Polynomial					Legendre-Chebyshev				
	[4,1]	[5,2]	[7,3]	[9,3]	[10,4]	[4,1]	[5,2]	[7,3]	[9,3]	[10,4]
2	0.656	0.889	1.004	0.998	0.999	0.656	0.889	1.004	0.998	1.000
3	0.620	0.989	1.001	0.999	1.002	0.620	0.989	1.001	1.000	1.002
4	0.817	1.014	1.002	1.000	1.002	0.817	1.014	1.002	1.000	1.002
5	0.841	1.007	1.003	1.001	1.002	0.841	1.007	1.003	1.001	1.002
20	0.746	0.995	1.001	1.002	0.997	0.746	0.995	1.001	1.010	1.002

6.2 Distortion analysis

Now consider the six-element beams shown in Fig. 5, with one end fixed. A mesh distortion analysis is made with three load cases presented, being $\boldsymbol{P_X} = \boldsymbol{P_Y} = \boldsymbol{P_Z} = 1$, $E=10^{-7}$, $v = 0.3$. The measured displacements in the center of the loaded face are then compared with the theoretical displacement results from beam theory, which are $\delta_X = 0.00003$, $\delta_Y = 0.1081$ and $\delta_Z = 0.4321$. Each mesh was evaluated with approximation degrees [4,1], [5,2], [7,3], [9,3] and [10,4]. Table 2 comprises the results of the homogeneous harmonic non-orthogonal functions, and Tab. 3 of the Legendre-Chebyshev functions.

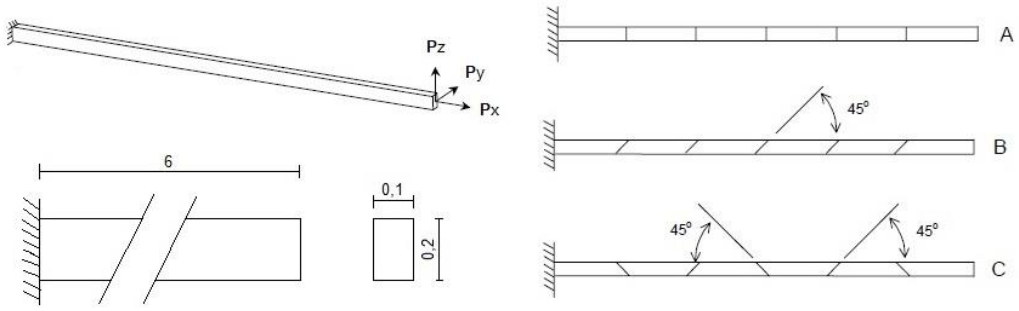

Figure 5. (Left) Beam dimensions and load cases. (Right) Meshes used in the distortion analysis.

Table 2. Distortion analysis of clamped beam using non-orthogonal harmonic polynomial approximation functions.

	Px			Py			Pz		
	A	B	C	A	B	C	A	B	C
[4,1]	1.000	1.000	1.000	0.158	0.791	0.855	0.173	0.091	0.087
[5,2]	1.000	1.000	1.000	0.995	0.995	0.994	0.995	0.993	0.993
[7,3]	1.000	1.000	1.000	1.000	1.000	1.000	0.998	0.998	0.998
[9,3]	0.999	0.999	0.999	0.999	0.999	0.999	0.997	0.997	0.997
[10,4]	0.999	1.004	0.999	0.999	0.999	0.999	0.998	0.998	0.998

Table 3. Distortion analysis of clamped beam using orthogonal Legendre-Chebyshev approximation functions.

	Px			Py			Pz		
	A	B	C	A	B	C	A	B	C
[4,1]	1.000	1.000	1.000	0.158	0.790	0.802	0.173	0.090	0.082
[5,2]	1.000	1.000	1.000	0.995	0.994	0.994	0.995	0.993	0.993
[7,3]	1.000	1.000	1.000	1.000	1.000	1.000	0.998	0.998	0.998
[9,3]	0.999	0.999	0.999	0.999	0.999	0.999	0.997	0.997	0.997
[10,4]	0.999	0.999	0.999	0.999	0.999	0.999	0.998	0.998	0.998

7. CONCLUSION

It is possible to see that both orthogonal and non-orthogonal trial functions had a very similar convergence rate for the proposed degrees of approximation, and very good results even with few elements and lower degrees of approximation. Very good results were also found within the distortion test applying the non-orthogonal homogeneous

harmonic polynomials. From these results it is possible to see that despite the fact the proposed approximation function produces a solving system with lower sparsity, their results are of the same level as the usually used orthogonal functions. Computational advancements in the last decades made possible to work with increasingly large matrices and solving systems, opening new possibilities for the study of novel approximation functions.

8. ACKNOWLEDGEMENTS

This study was financed in part by the Coordenação de Aperfeiçoamento de Pessoal de Nível Superior – Brasil (CAPES) – Finance Code 001

9. REFERENCES

Bussamra, F. L., Pimenta, P. d. M., Freitas, J. A. T. d., "Hybrid-trefftz stress elements for three-dimensional elastoplasticity", *Computer Assisted Methods in Engineering and Science* 8 (2001) 235–246.

Bussamra, F.L.d.S., Lucena Neto, E. and Rodrigues, M.A.C., 2016. "Simulation of stress concentration problems in laminated plates by quasi-trefftz finite element models". *Latin American Journal of Solids and Structures*, Vol. 13, No. 9, pp. 1677–1694.

Bussamra, F., Neto, F., Ponciano, W., "Simulation of stress concentration problems by hexahedral hybrid-trefftz finite element models", *Computer Modeling in Engineering & Sciences* 99 (3) (2014) 255–272.

Bussamra, F., Neto, E. L., Raimundo Jr, D., "Hybrid quasi-trefftz 3-d finite elements for laminated composite plates", *Computers & Structures 92* (2012) 185–192.

Cao, C., Qin, Q.-H., Yu, A., "Micromechanical analysis of heterogeneous composites using hybrid-trefftz fem and hybrid fundamental solution-based fem", *Journal of Mechanics* 29 (4) (2013) 661–674

Cong, T. T., Steven, G., "On the representation of elastic displacement fields in terms of three harmonic functions", *Journal of Elasticity* 9 (3) (1979) 325–333.

de Argôlo, H. S. D., Proença, S. P. B., "Splitting method and hybrid-trefftz formulation for multisite damage analysis in two-dimensional domains", *International Journal of Solids and Structures* 104 (2017) 50–64.

de Veubeke, B. F., "Diffusive equilibrium models", *BM Fraeijs de Veubeke memorial volume of selected papers* (1980) 569–628.

de Souza, C.O. and Proença, S.P.B., 2011. "A hybrid-trefftz formulation for plane elasticity with selective enrichment of the approximations". *International Journal for Numerical Methods in Biomedical Engineering*, Vol. 27, No. 5, pp. 785–804.

Eubanks, R., Sternberg, E., "On the completeness of the boussinesq-papkovich stress functions", *Journal of Rational Mechanics and Analysis* 5 (5) (1956) 735–746.

Freitas, J. T. d., Almeida, J. M. d., Pereira, E. R., "Non-conventional formulations for the finite element method", *Computational Mechanics* 23 (5-6) (1999) 488–501.

Freitas, J. T. d., Bussamra, F., "Three-dimensional hybrid-trefftz stress elements", *International Journal for Numerical Methods in Engineering* 47 (5) (2000) 927–950.

Freitas, J. T. d., Ji, Z.-Y., "Hybrid-trefftz finite element formulation for simulation of singular stress fields", *International Journal for Numerical Methods in Engineering* 39 (2) (1996) 281–308.

Freitas, J. T. d., Ji, Z.-Y., "Hybrid-trefftz equilibrium model for crack problems", *International Journal for Numerical Methods in Engineering* 39 (4) (1996) 569–584.

Freitas, J. T. d., "Formulation of elastostatic hybrid-trefftz stress elements", *Computer Methods in Applied Mechanics and Engineering* 153 (1-2) (1998) 127–151.

Fu, X.-r., Yuan, M.-w., Cen, S., Tian, G., "Characteristic equation solution strategy for deriving fundamental analytical solutions of 3D isotropic elasticity", *Applied Mathematics and Mechanics* 33 (10) (2012) 1253–1264.

Fu, Z.-J., Qin, Q.-H., Chen, W., "Hybrid-Trefftz finite element method for heat conduction in nonlinear functionally graded materials", *Engineering Computations* 28 (5) (2011) 578–599.

Hu, H., "The collected works of academician Hu Hai-Chang", *China Astronautic Publishing House, Beijing* (2008).

Kaczmarczyk, Ł., Pearce, C. J., "A corotational hybrid-trefftz stress formulation for modelling cohesive cracks", *Computer Methods in Applied Mechanics and Engineering* 198 (15-16) (2009) 1298–1310.

Karkon, M. "Hybrid-trefftz formulation for analysis of anisotropic and symmetric laminated plates", *Composite Structures* 134 (2015) 460–474.

Karkon, M., Rezaiee-Pajand, M., "Hybrid-trefftz formulation for analysis of thick orthotropic plates", *Aerospace Science and Technology* 50 (2016) 234–244.

Lee, M.G., Young, L.J., Li, Z.C. and Chu, P.C., "Combined trefftz methods of particular and fundamental solutions for corner and crack singularity of linear elastostatics". *Engineering Analysis with Boundary Elements*, Vol. 34 (2010), No. 7, pp. 632–654.

Mindlin, R., "Note on the galerkin and papkovitch stress functions", *Bulletin of the American Mathematical Society* 42 (6) (1936) 373–376.

Naghdi, P., Hsu, C., "On a representation of displacements in linear elasticity in terms of three stress functions", *Journal of Mathematics and Mechanics* (1961) 233–245.

Neuber, H. v.,"Ein neuer ansatz zur lösung räumlicher probleme der elastizitätstheorie. der hohlkegel unter einzel-19 last als beispiel", *ZAMM-Journal of Applied Mathematics and Mechanics/Zeitschrift für Angewandte Mathematik und Mechanik* 14 (4) (1934) 203–212.

Papkovich, P., "Solution générales des équations differentielles fondamentales d' elasticité exprimée par trois fonctions harmoniques", *Comptes Rendus Mathematique Academie des Sciences, Paris* 195 (3) (1932) 513–515.

Petrolito, J., "Vibration and stability of plates using hybrid-trefftz elements", *International Journal of Structural Stability and Dynamics* 4 (04) (2004) 559–578.

Petrolito, J., "Vibration and stability analysis of thick orthotropic plates using hybrid-trefftz elements", *Applied Mathematical Modelling* 38 (24) (2014) 5858–5869.

Pian, T. H., "Derivation of element stiffness matrices by assumed stress distributions", *AIAA journal* 2 (7) (1964) 1333–1336.

Pian, T. H., Tong, P., "Basis of finite element methods for solid continua", *International Journal for Numerical Methods in Engineering* 1 (1) (1969) 3–28.

Rezaiee-Pajand, M., Karkon, M., "Two efficient hybrid-Trefftz elements for plate bending analysis.", *Latin American Journal of Solids and Structures*, 9(1), (2012) 43-67.

Rezaiee-Pajand, M., Karkon, M., "Two higher order hybrid-Trefftz elements for thin plate bending analysis.", *Finite Elements in Analysis and Design*, 85, (2014) 73-86.

Sokolnikoff, I.S., "Mathematical theory of elasticity", *McGraw-Hill book company*, (1956).

Wang, M. Z. "Advanced Theory of Elasticity.", *Chinese, Peking University Press, Beijing* (2002).

Wang, M.-Z., Xu, B.-X., Zhao, Y.-T., "General representations of polynomial elastic fields", *Journal of Applied Mechanics* 79 (2) (2012) 021017.

10. RESPONSIBILITY NOTICE

Felipe Alvarez Businaro and Flávio Luiz da Silva Bussamra are the only responsible for the printed material included in this paper.